Chapter 21

Two-Wave Mixing in Organic-Inorganic Hybrid Structures for Dynamic Holography

Vera Marinova, Shiuan Huei Lin and Ken Yuh Hsu

Additional information is available at the end of the chapter

http://dx.doi.org/10.5772/67190

Abstract

The chapter reviews recent progress of two-wave mixing in a novel organic-inorganic hybrid structures that combine essential properties as large anisotropy and strong birefringence, typical for organics with the excellent photosensitivity and photoconductivity of inorganics into single, compact devices. Depending on the designed assembly and operation principle, the proposed structures can record dynamic holographic gratings at Raman-Nath or Bragg regimes of diffraction, respectively. When the two beams interact in a structure based on a photoconductive material and birefringent layer (usually liquid crystal), the beam coupling with high amplification values occur in a liquid crystal layer, however, the fringe period of recorded holograms is limited to few μm scale. In contrast, when the two beams interact in a structure based on a photorefractive material and birefringent layer, the beam-coupling occurs in both composites, due to the surface activated photorefractive effect. The prime significance of the later structure is the ability to act as a holographic grating at Bragg regime allowing sub-micron spatial resolution. Moreover they are easy and simple to fabricate where the processes are all optically controlled. The above examples open scenarios to design new devices that meet the latest requirements of 3D display technologies and optical information processing.

Keywords: liquid crystals, inorganic crystals, beam amplification, Raman-Nath diffraction, Bragg diffraction, photorefractive effect, space-charge field

1. Introduction

The demand to develop advanced functional devices with fast operation speed, high memory capability, submicron spatial resolution and low energy consumption continuously tends to increase. For example, to reach a wide viewing angle, the pixel pitch of the recording media

needs to be comparable or smaller than the wavelength of the light. Another approach is to design all optically controlled devices for light control and manipulation. All these features make the combination between outstanding properties as large anisotropy and strong birefringence typical for organics (offering easy processing, large structural flexibility and low cost) with the excellent photosensitivity and photoconductivity of inorganic materials (providing mechanical stability and energy gap manipulation) attractive to design single, compact structures with enhanced functionality. Moreover, an emergent need of devices sensitive at the near-infrared spectral range (the required illumination for biological and medical samples) is of particular importance for biomedical sensing and with significant impact for the society. In that aspect, the holography, due to its unique nature, is expected to play an essential role.

The following chapter is focused on the two-wave mixing in organic-inorganic hybrid structures and dynamic holography recording resulting to formation of light-induced gratings. The two-wave mixing (denoted also as a two-beam coupling) takes place in a variety of non-linear media as photorefractive materials (the photorefractive effect refers to refractive index modulation in response to light), third-order non-linear media (as Kerr media) or semiconductor amplifiers. The two-wave mixing is expressed by two beam interactions, forming an interference pattern, which is characterized by periodic spatial variation of the light-intensity distribution. Its main significance is the ability of unidirectional optical energy exchange between the two beams (gain amplification) allowing weak beam to grow exponentially with the distance, which opens various opportunities for designing a new structures and elements for practical realizations.

Depending of the organic-inorganic hybrid structure design and in more particular how the inorganic material control the dynamic grating formation, they can operate at Raman-Nath or Bragg match regime of diffraction:

i) Generally, the organic-inorganic structures are assembled by photoconductive material (usually inorganic crystal) and birefringent material (liquid crystal [LC] or polymer dispersed liquid crystal [PDLC]). Their operation principle relays on electro-optically controlled birefringence of the liquid crystal molecules that allows spatial modulation of the amplitude or the phase of incident beam. In such configuration, the inorganic crystal serves as a photoconductive layer, which controls the LC molecules alignment and allows subsequent light modulation. As a result, the two-wave mixing happens in a LC layer with very high amplification values; however, the fringe period of the recorded holograms is limited to few micrometer scales (Raman-Nath regime of diffraction). Usually, this type of hybrid structures is known as electro-optically controlled devices.

ii) Recently, a novel type of organic-inorganic structures has been proposed assembled by photorefractive material and birefringent layer (LC or PDLC). Their operation principle relays on surface-activated photorefractive effect and more specific on the photo-generated space charge field, acting as a driving force for LC molecules reorientation and subsequently the refractive index modulation. The prime significance is the fact that the two-wave mixing happens in both photorefractive and birefringent layers, where the charge

carrier migration, high-trap density and space-charge field come from the inorganic substrate, whereas the beam amplification is provided by the LC layer. As a result, the proposed hybrid structures act as dynamic holographic grating at Bragg match regime allowing sub-micron spatial resolution. Moreover, the above configuration is easy and simple to fabricate (no need of conductive layer deposition [and in a case of PDLC, no need of alignment layers and polarizers]), and all the processes are controlled only by the action of light. Therefore, they are noted as all optically controlled hybrid devices.

The chapter is organized as following: at the beginning, a brief introduction of two-wave mixing and gain amplification phenomena as a consequence from the non-linearity of photorefractive effect will be reviewed. The main significances of the optical energy exchange and phase shift between the interference pattern and refractive index grating are discussed. Next, the two-wave mixing in two types of organic-inorganic hybrid structures (electro-optically controlled and all optically controlled) will be presented and compared. Examples as optically addressed spatial light modulation devices; in dynamic holography and image processing are demonstrated and discussed. In concluding remarks, further prospective to design varieties of novel all optically controlled hybrid devices will be discussed.

2. Raman-Nath and Bragg match regimes of diffraction

The interaction between two coherent laser beams inside the photosensitive material generates a light-intensity fringe pattern of bright and dark regions (sinusoidal light intensity pattern) expressed by [1, 2]:

$$I(x) = I_0 [\, 1 + m\cos(Kx) \,] \tag{1}$$

where I_1 and I_2 are the intensities of both beams, I_0 is the total intensity $I_0 = (I_1 + I_2)$ and m is the light modulation, $m = 2\frac{(I_1 I_2)^{1/2}}{I_0}$.

The created diffraction grating is defined by the two interfering beams and their spatial coordinates, determined by the grating wave vector $K = 2\pi/\Lambda$ and the spatial fringe period $\Lambda = \frac{\lambda}{2\sin\theta}$, where λ is the wavelength, and θ is the external half angle between of the intersection beams. After propagation through the medium, the same beams diffract from the holographic grating, which they formed.

The light diffraction phenomenon from periodic structures has been extensively discussed in the past and defined to two regimes of diffraction: (i) Raman-Nath regime (when several diffracted waves are produced named thin grating) and (ii) Bragg matched regime (when only one diffracted wave is produced named thick or volume grating) [1, 2].

Briefly, in Raman-Nath regime, after interacting with the grating, the incident beam is split into several beams resulting in different orders of diffraction (see **Figure 1(a)**). As a consequence, there are several diffracted waves produced 0, ±1, ±2, ±3,… ±m, which correspond

to the wave vectors k, k ± **K**; k ± 2**K**; k ± m**K**, where k is the wave number of light beam in the medium and **K** is the grating wave vector. The diffraction efficiency for the Raman-Nath diffraction is given by [1]

$$\eta_m = J_m^2(\delta) = J_m^2\left(\frac{2\pi Ln}{\lambda cos\theta}\right) \tag{2}$$

where $J_m(\delta)$ is the amplitude of the mth order diffracted beam, expressed by Bessel's function (δ is expression of modulation index corresponding to the multiple scattered orders), n is the refractive index of the medium and L is the interaction thickness [3, 4].

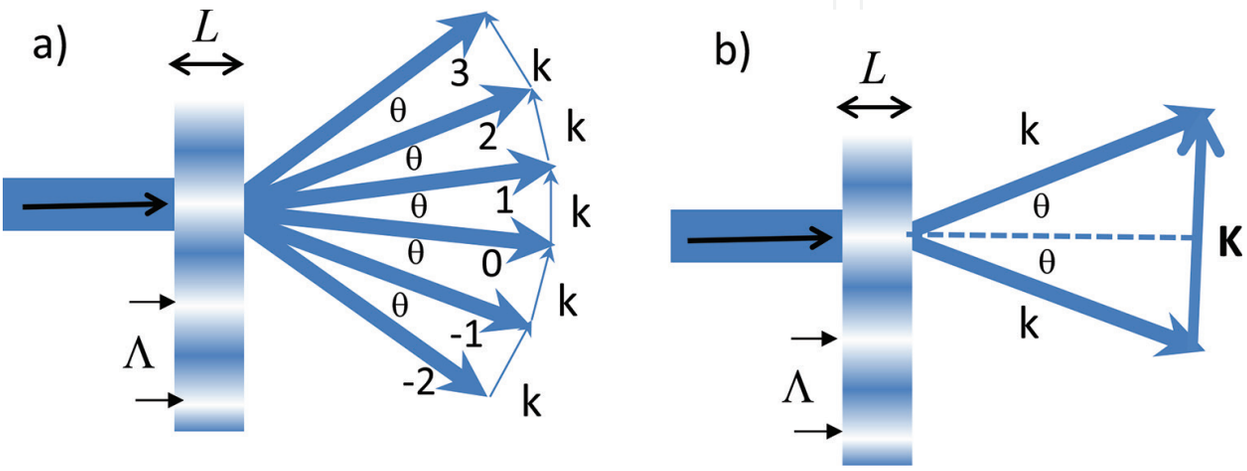

Figure 1. Raman-Nath (a) and (b) Bragg matched regime of diffraction [1].

In a Bragg regime, after interacting with the grating, only one diffracted wave is produced, and the diffraction occurs only when the incident angle satisfies the Bragg conditions [1–4] (both the energy and momentum are conserved)—see **Figure 1(b)**.

The simplified diffraction efficiency (in case of transmission type, sinusoidal phase grating) is given by [2]

$$\eta = sin^2\left(\frac{\pi nL}{\lambda cos\theta}\right) \tag{3}$$

Generally, Klen-Cook dimensionless parameter has been accepted as distinguishing factor between the Raman-Nath or Bragg regimes of operations, defined by [5]:

$$Q = \frac{2\pi\lambda L}{n\Lambda^2} \tag{4}$$

Although this parameter has been extensively used as a criterion which regime to apply ($Q \leq 1$ for Raman-Nath or $Q > \sim 1$ for the Bragg-matched regime), it requires several limitation of the grating strength [6].

http://dx.doi.org/10.5772/67190

3. Two-wave mixing and optical gain amplification in photorefractive media

The two-wave mixing appears in variety of non-linear media, and owing to its wide range of applications, it has been extensively studied in a past [7–10]. In general, the two-wave mixing is described by two beam interactions inside the photosensitive material, forming a light interference pattern (index grating). As a result, the two beams diffracted by the index grating they created in a way that in one direction, the diffracted and transmitted intensities provide constructive interference (with higher resultant intensity), whereas in the other direction, the beams experience destructive interference (with lower resultant intensity). Thus, the most significant importance of the two-wave mixing is the energy exchange between the two interacting beams.

The light illumination in a photosensitive material causes generation of free charge carriers and their redistribution from the regions of high intensity to those of low intensity (see **Figure 2**). This net migration leads to inhomogeneous charge distribution and accumulation of an internal electric field known as a space charge field E_{sc}. Actually, this space charge field is of key importance for the photorefractive effect and can play significant role for the LC molecules reorientation as discussed further.

Briefly, the space charge field is expressed by the following set of well-known equations [1, 7, 8]:

$$\frac{\partial N}{\partial t} - \frac{\partial N_D^i}{\partial t} = \frac{1}{e} \nabla \cdot J \tag{5}$$

$$\frac{\partial N_D^i}{\partial t} = \left(N_D - N_D^i\right) sI - \gamma_R N N_D^i \tag{6}$$

$$\mathrm{J} = J_{drift} + J_{diffusion} = eN\mu E_{sc} + k_B T\mu \nabla N \tag{7}$$

$$\nabla \cdot \varepsilon E_{sc} = \rho(r) = -q\left(N + N_A - N_D^i\right) \tag{8}$$

where e is the electron charge, N is density of main charge carriers, N_D is total donor density, $N_D{}^i$ is ionized donor density, N_A is density of acceptors, s is absorption cross section of excitation, γ_R is ionized trap recombination rate, μ is mobility, J is current density, ρ is charge density, ε is dielectric constant, k_B is Boltzmann constant and T is the temperature. In Eqs. (5)–(8), Eq. (5) is the rate equation of the main carriers density; Eq. (6) is the rate equation of ionized donors (the first term is the rate of main carriers generation and the second term is the rate of the trap capture); Eq. (7) is the current density equation (if neglect the photovoltaic effect); and Eq. (8) is the Poisson equation.

The first term in Eq. (7) is expressed by the drift of the charge carriers due to the space charge field E_{sc} and the second term is a diffusion, due to the gradient of the charge carrier density, expressed by the diffusion length $L_D = \left(\frac{E_D}{K}\mu\tau_D\right)^{1/2}$; where $\tau_D = \frac{e\Lambda^2}{4\pi^2\mu k_B T}$ is the diffusion time and

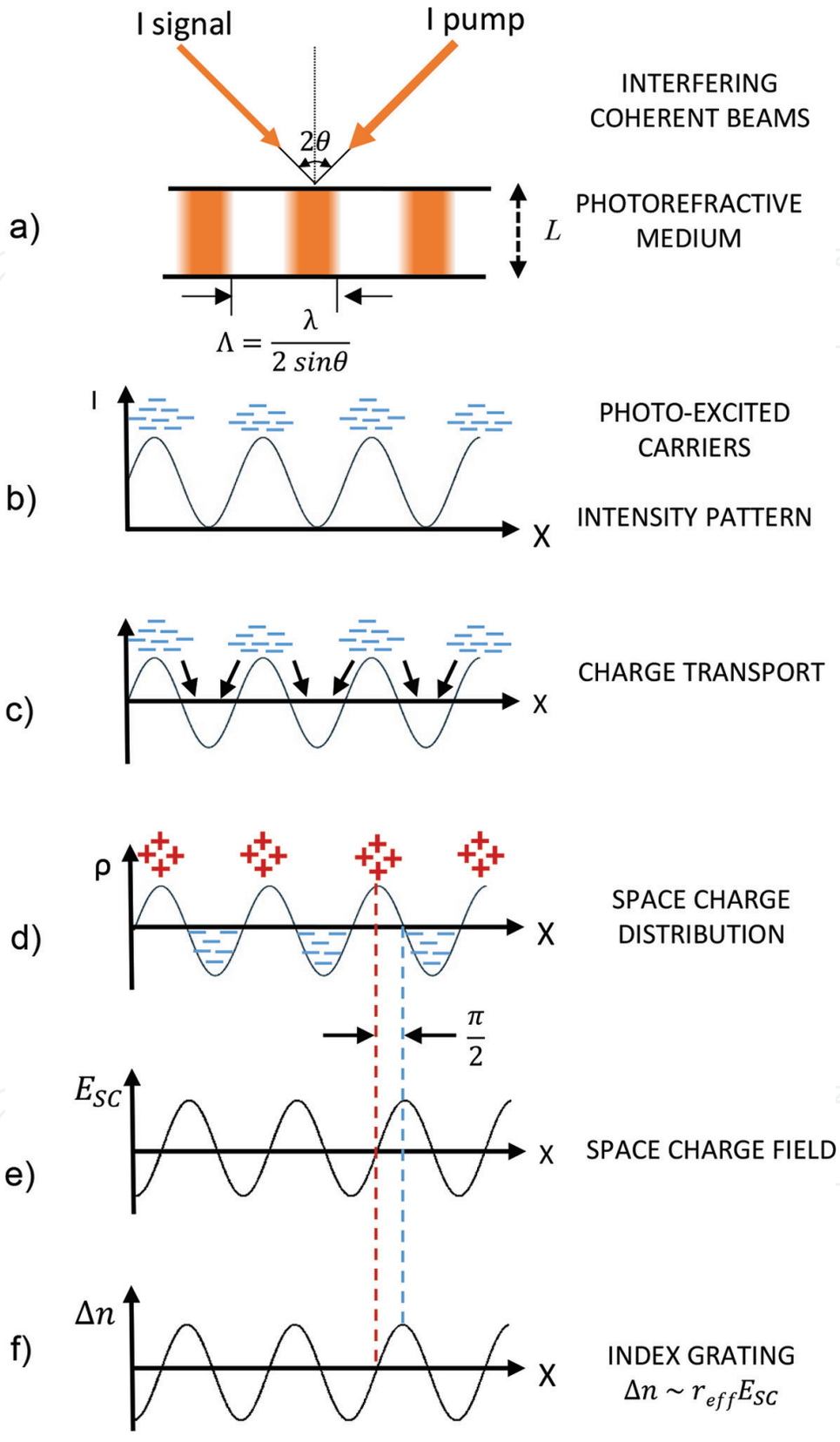

Figure 2. The photorefractive effect: (a) two-beams interference; (b) photo excitation process (intensity pattern); (c) charge transport; (d) space-charge distribution; (e) space-charge field and (f) index grating formation.

$E_D = \frac{KD}{\mu} = \frac{Kk_B}{E}T$ is the diffusion field. The magnitude of the E_{sc} depends on several materials parameters, among which the Debye screening length $L_D = \left(\frac{\varepsilon\,\varepsilon_0}{N_{eff}}\frac{k_B T}{e^2}\right)^{\frac{1}{2}}$ and effective trap density $N_{eff} = \frac{\left(N_D - N_D^i\right)N_D^i}{N_D}$.

In liquid crystals, the drift is the dominant mechanism for the charge carrier migration due to the small trap density of organics. In contrast, the diffusion is the dominant mechanism for inorganic materials and the rate at which the recombination happens determine how far the main charge carrier diffuse and how strong is the refractive index modulation. For instance, inorganic crystals offer several orders of magnitude higher concentration of effective trap density in contrast to the LCs and therefore are able to support formation of the small grating spacing and Bragg match regime of diffraction as will be discussed later.

As a result of charge migration and redistribution, the space charge field in combination with the electro-optic effect modulates the refractive index of the media via the Pockel's effect [1, 8, 9]:

$$\Delta\left(\frac{1}{n^2}\right) = r_{ijk}E_{sc} \tag{9}$$

where r_{ijk} is the electro-optic coefficient.

The recorded refractive index grating can diffract light, with the diffraction pattern reconstructing the light-intensity pattern, originally stored in the media. Therefore, the index grating created in the photorefractive material is a "volume phase hologram", which can be written and erased by light, making photorefractive materials fully reversible. Thus, the photorefractive materials have the ability to detect and store spatial distributions of optical intensity in the form of spatial patterns of modulated refractive index.

The most significant consequence from the photorefractive effect is the phase shift between the light-intensity pattern and internal spatial pattern where the later one shifted in respect to the intensity distribution by $\pi/2$ period (see **Figure 2**). This $\pi/2$ phase shift induces an optical energy exchange between the two interacting beams (beam amplification) and refers the photorefractive effect as non-local, non-linear effect [2, 7, 8]. Therefore, when two interfering beams have different intensities noted as respectively I_s "signal" beam (with lower intensity) and I_p "pump" beam (with higher intensity), due to destructive and constructive interference, the unidirectional transfer of optical energy allows a weak beam to grow exponentially with the distance. As a result, at the exit of the medium, the signal beam is not only amplified but also experienced a non-linear phase shift.

The interaction between the two coherent laser beams inside the photosensitive material (assuming the grating wave vector **K** directed along the x axis) gives the total electric field of the two incident beams

$$E = A_1 exp\left[i\left(k_1 . r - \omega_1 t\right)\right] + A_2 exp\left[i\left(k_2 . r - \omega_2 t\right)\right] \tag{10}$$

(where $A_{1,2}$ are the beam amplitudes; κ_1 and κ_2 are the wave vectors $\mathbf{K} = |\kappa_2 - \kappa_1|$; r and t are spatial and temporal coordinates; ω_1 and ω_2 are the angular frequency ($\Delta\omega = \omega_2 - \omega_1$) and δ is the frequency detuning between the two beams) and generates a light-intensity fringe pattern of bright and dark regions (sinusoidal light-intensity pattern) described as [1, 7, 8]:

$$\mathrm{I} = \left|A_1\right|^2 + \left|A_2\right|^2 + \left\{A_1 A_2^* exp[i(-Kx + \delta t)] + c\,.\,c.\right\} \tag{11}$$

In fact, Eq. (11) represents the spatial variation of the intensity pattern inside the photosensitive media that generates and redistributes the charge carriers and accumulates the space charge field.

As a result, the refractive index grating, summarized by Refs. [8, 9], can be written by:

$$\Delta\mathrm{n} = n_0 + \left\{\Delta n_0 A_1 A_2^* exp[i(-Kx + \delta t + \Phi)] + c\,.\,c.\right\} \tag{12}$$

where Φ is the phase difference between the refractive index grating and interference pattern, n_0 is the refractive index without the light and the Δn_0 is amplitude of index modulation.

By using the couple-mode theory [1, 11], the quantitative measure of the beam-coupling is expressed by the gain coefficient Γ [1, 8, 9]

$$\Gamma = \frac{2\pi\Delta n_0}{\lambda cos\theta}\sin\phi \tag{13}$$

Experimentally, the gain coefficient can be measured by the ratio

$$\Gamma = \frac{1}{L}\ln\left(\frac{I_s' I_p}{I_s I_p'}\right) \tag{14}$$

where $I'_{p(s)}$ is the transmitted intensity of the pump (signal) beam with a coupling, and $I_{p(s)}$ is the transmitted beam intensity without coupling.

The general parameter characterizing the gain is the gain amplification G, given by:

$$G = \frac{1}{L} log_e[\Gamma] \tag{15}$$

where L is the interaction length of the media.

In last decades, the two-beam coupling effect has been widely investigated in varieties of organic and inorganic compounds [1, 7–13]. In terms of organics, the electro-optic response and the build-up of a refractive index grating in liquid crystals arise from the reorientation of LCs molecules due to an induced space charge field. This effect is known as "orientational photorefractive effect" or "photorefractive-like effect" [12]. For most applications, an external electric field needs to be applied along the grating vector direction, since the drift is the dominant mechanism for the charge migration in LC systems. LCs or PLDCs provide very

high amplification gain (up to 2600 cm^{-1} [14]); however, the large grating spacing and small trap density, typical for organics restricted the two-beam coupling to the Raman-Nath regime of diffraction. Therefore, due to the multiple orders of diffracted beams, which accumulate the optical losses, the energy lost limits many of the practical uses.

In terms of inorganic crystals, the direction of the optical energy transfer depends on the sign of the electro-optic coefficient and the sign of the main charge carriers. Up to now, the highest gain coefficient (over 100 cm^{-1}) has been reported in Fe-doped $LiNbO_3$ crystal due to its large refractive index modulation $\Delta n \sim 2 \times 10^{-3}$ [15]. Relatively high beam amplification has been achieved in SBN and $BaTiO_3$ inorganic crystals [7, 10]. In $Bi_{12}(M = Si,Ti)O_{20}$ sillenite crystals, the gain coupling is much lower due to the smaller values of the electro-optical coefficient, restricted by the cubic symmetry [16]. However, doped sillenite crystals offer the potential for high-carrier mobility (high photoconductivity) and together with the high-trap density can compensate the small-trap density of LCs when combined into a hybrid structure to support the fine grating spacing and to fulfil the requirements for Bragg-matched regime of diffraction. Furthermore, by selecting the photorefractive substrate sensitivity, the operation interval of the proposed hybrid devices can be easily adjusted. Moreover, doping sillenites with transition metal elements significantly improve their sensitivity and response time at near-infrared spectral range [17–22].

4. Organic-inorganic hybrid structures operating at Raman-Nath regime of diffraction

4.1. Organic-inorganic structure design and principle of operation

This type of organic-inorganic hybrid structure consists of photoconductor substrate (usually an inorganic crystal plate with 0.4–0.6 mm thickness) and electro-optic layer (few microns thickness) arranged into a cell, supported by a glass substrate from another side (see the schematic diagram at **Figure 3(a)**). Selected inorganic crystals stand as photoconductors, whereas a LC layer is used

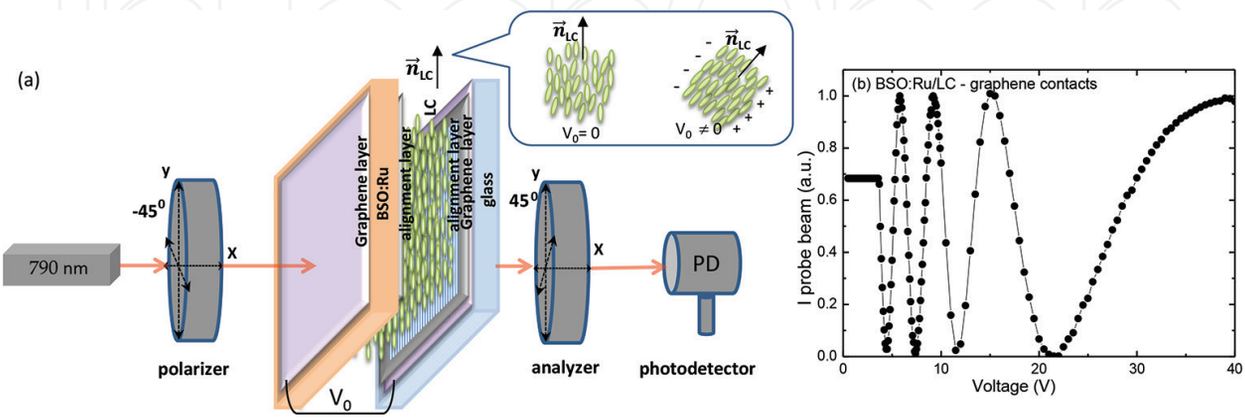

Figure 3. (a) Experimental set-up for voltage-transmittance measurements. The hybrid structure is placed between two crossed polarizes making an angle of 45° with respect to the transmission axis of the polarizer (b) Example of Voltage-Transmittance dependence for BSO:Ru/LC structure with graphene-based electrodes.

as electro-optic material. The proposed configuration is also known as optically addressed spatial light modulator (OASLM) structure. As the read-out process can provide an optical gain, the OASLMs have been also considered as a liquid crystal light valve (LCLV) devices.

$Bi_{12}SiO_{20}$ (BSO) and $Bi_{12}TiO_{20}$ (BTO) crystals are among the perfect components for OASLM devices due to their remarkable photoconductivity and high charge carrier mobility. For a first time, non-doped BSO crystal was assembled with a LC layer into a LCLV, working at transmittance mode by Aubourg et al. [23]. Later on, several devices operating at visible spectral range have been demonstrated [24–26]. Other preferable photoconductor substrates are semiconductors as a-Si:H, crystalline silicon, gallium arsenide, indium phosphate and cadmium tellurite [27, 28]. Usually, transparent indium tin oxide (ITO) conductive layers are preliminary deposited on the outer side of the photoconductive plate and the inner side of glass substrate and coated with polyvinyl alcohol (PVA) for planar alignment of the LC molecules. Recently, owing to the ITO limited transparency at near infrared spectral range and increased cost because of the Indium scarcity in the nature, ITO has been successfully replaced with graphene conductive layers, and several graphene-based devices have been successfully demonstrated [29, 30].

The operation principle of OASLM device relays on the electro-optically controlled birefringence of the LCs molecules where the high sensitivity and photoconductivity comes from the photoconductive plate and high birefringence is provided by the LC layer [2, 31]:

(i) when an external AC voltage (V_0) is applied across the device (**Figure 3(a)**), the applied voltage acts through the photoconductor substrate because of its high resistance. Since the LCs molecules have different polarizability along their long and short axis, the applied voltage induces a dipole moment in the LC layer, which affects the LC molecules orientation, and they follow the direction of the applied electric field. As the LC nematic phase is characterized by a long-range orientation order, all the LC molecules tend to align along the nematic LC director $\hat{n}_{LC}$. Therefore, when the structure is placed between the crossed polarizers, "on" and "off" illumination states are obtained (**Figure 3**).

(ii) Illumination with the input pump beam activates the photoconductor substrate, and charge carriers are generated at a rate proportional to the pump intensity. Owing to the crystal's high photoconductivity and high dark resistivity, the charge separation decreases the voltage across the photoconductor, and it reduces its impedance. As a consequence, the accumulated voltage is transferred into the LC layer, resulting in a LC molecular reorientation.

Owing to the LC's anisotropy, the output beam obtains a phase shift

$$\varphi = \frac{2\pi}{\lambda}\left(n_e - n_0\right)L \tag{16}$$

which is a function of the applied voltage V_0 and the pump light intensity I:

$$I = \frac{1}{2}sin^2\frac{\Phi}{2} = \frac{1}{2}sin^2\left[\frac{\pi\left(n_e - n_0\right)L}{\lambda}\right] \tag{17}$$

http://dx.doi.org/10.5772/67190

where L is the LC thickness, n_e and n_0 are refractive indexes for a beam polarized along the long or short molecular axis $\Delta n = n_e(I_p) - n_0$ and Φ is the phase retardation [2]. This allows spatial modulation of the amplitude or phase of the incident beam at the exit of device (see **Figure 4(a)**). During the full range, the reorientation angle of the LC molecules can vary from 0 to $\pi/2$, producing a phase shift of several π.

Figure 3 illustrates the experimental set-up and the typical Freedericksz transition characteristics of BSO:Ru/LC device with graphene electrodes, operating at 1064 nm. The modulation behaviour supports the LC molecules alignment in the direction of an applied AC voltage across to the cell. **Figure 4** shows the phase modulation set up and phase difference for the same BSO:Ru/LC device at fixed voltage of 4 V (according to the results at **Figure 3(b)**). The probe-pump intensity dependence is presented as inset at **Figure 4(b)**.

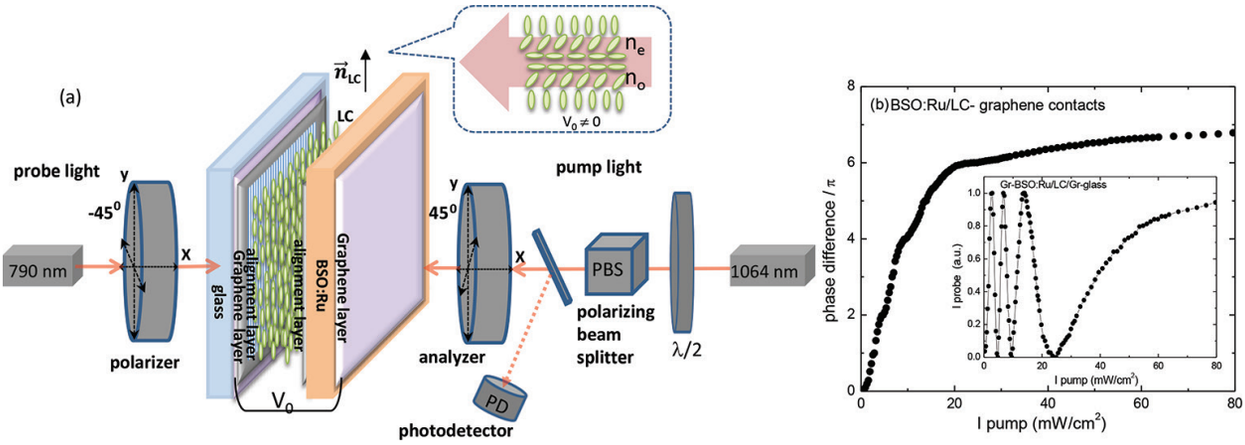

Figure 4. (a) Experimental set-up for phase shift measurements and (b) Phase difference as a function of a pump light intensity (fixed at 4V according to the results from figure 3(b)) for BSO:Ru/LC device. Inset graph shows the probe-pump intensity dependences.

Obviously, the light-induced modulation formed in the photoconductive substrate is the driving force, which affects the LC molecules realignment and spatially modulates the refractive index of LC layer.

4.2. Two-wave mixing and Raman-Nath regime of diffraction

For a first time, energy transfer using two-wave mixing has been demonstrated by Brignon et al. [32] in a device assembled by BSO photoconductive crystal and LC layer. The recorded holographic gratings were not typical local dynamic grating as generally supposed to be created from the photoconductive substrate. The two-beam interaction has been described as a diffraction of the two beams on a fixed thin local grating (the index grating formed in LC), which is pinned to the conductivity grating [32]. Since the photoconductive and the electro-optic regions are separate, the photo-induced grating is not modified by the interacting beams during their propagation in the LC layer. Later on, beam amplification in LCLV devices has been verified and reported in several papers [19, 21, 23–26, 33]. Recently, significant gain

amplification values have been obtained in hybrid structures based on semiconductor crystals as GaAs doped with Cr [33, 34] or CdTe [35].

The interference between the pump and signal beam, expressed by their amplitudes $E_p \exp\,[\,i(\kappa_p \cdot r - \omega_p \cdot t)\,]$ and $E_s \exp\,[\,i(\kappa_s \cdot r - \omega_s \cdot t)\,]$, produced an intensity fringe pattern that induces a space-charge distribution and consequently a molecular re-orientation pattern in the LC layer. The interaction creates a refractive index grating with the same wave vector K, and as a result, the two beams diffracted by the photo-induced grating with spatial grating period of $\Lambda = 2\pi/K$.

In these hybrid structures, the active layer is the LC layer; therefore, the interaction length is sufficiently thin to satisfy the energy and momentum conservation before exiting the medium [1, 2]. As a result, the two-beam coupling occurs in a Raman-Nath regime of diffraction (the LC layer is much thinner in comparison with the grating spacing $L << \Lambda$). Consequently, the phase grating recorded in the LC layer acts as a thin hologram with a multiple output beams.

A detailed analysis of the two-wave mixing and expression of the zero and m-output diffracted orders is given in Ref. [24] where the evolution of the amplitude of the refractive index grating and relaxation dynamic of the LC molecules orientation has been considered, using the couple-wave theory [1, 11]. We note that the output signal beam according to Refs. [24, 36] can be written in a form:

$$E_{output} = \sqrt{G\,I_s}\,\exp(i\phi)exp\left[i\left(k_s\,.\,r - \omega_s\,t\right)\right] + c\,.\,c. \tag{18}$$

where G is the gain amplification and ϕ is the non-linear phase shift.

Figure 5 demonstrates the two-wave mixing in BTO:Rh/LC hybrid structure using 1064-nm diode laser. The right side of **Figure 5** supports the Raman-Nath diffraction with several diffracted beams (0, ±1, ±2,…) at the output of the hybrid device, detected on the infrared view card.

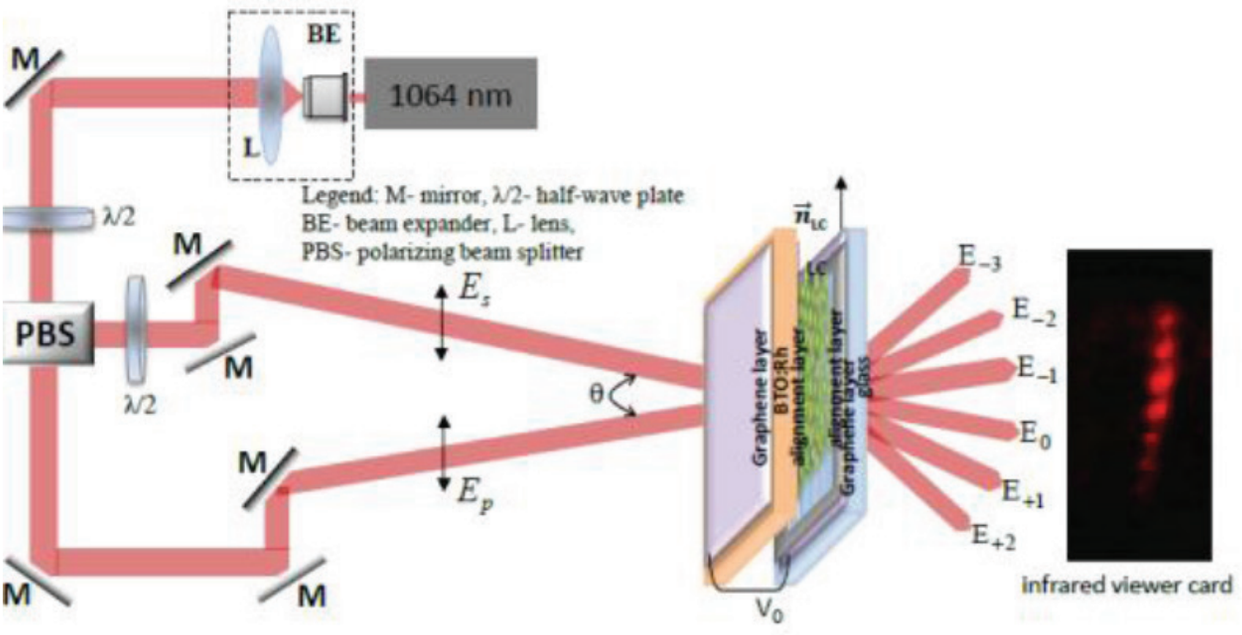

Figure 5. Two-wave mixing at Raman-Nath regime of diffraction (E_s and E_p are the amplitudes of the pump and signal beams) allowing high-gain amplification values (LC layer acts as thin hologram) at 1064 nm. Right side: Raman-Nath orders observed on a view card for BTO:Rh/LC device with graphene electrodes.

Experimentally, the gain parameter G has been measured by monitoring the intensities of two interfering beams as $G = I_0/I_s$, where I_s is the input signal intensity (without pump light) and I_0 is the amplified signal after the device. For example, at an interaction angle of 2.5°θ (12-μm grating period), the gain amplification for BTO:Rh/LC structure is $G = 4.1$ at 1064 nm. The gain coefficient of $\Gamma \sim 1180$ cm^{-1} has been calculated by the relation $I_{(0)} = I_{(s)}e^{\Gamma L}$, which is among the highest value reported until now for hybrid devices, operating at near infrared spectral range. Very recently, a gain amplification of 17 has been achieved at GaAs-based hybrid structure at 1064 nm with optimized thickness of the LC layer [33].

4.3. Applications

Based on the ability to record dynamic phase holograms, the reviewed electro-optically controlled structures found applications as optically addressed spatial light modulator devices, light-valve structures, to control the fast and slow components of light, in adaptive interferometry and metrology, and so forth [33–37].

When the address beam (incoherent image) is projected into photoconductive substrate, due to its high photoconductivity and high dark resistivity, the crystal reduces its impedance and accumulated voltage is transferred to the LC layer, resulting in LC molecular reorientation. Hence, the intensity distribution of the address beam in the photoconductor has a subsequent connection with the voltage distribution in the LC layer. This is the way how the "optical addressing" is realized. Consequently, when the two interfering beams intersect inside the hybrid structure, dynamic phase holograms can be addressed into the liquid crystal layer.

Based on the phase modulation ability, an evolution of image propagating on BTO:Rh/LC device is demonstrated. **Figure 6** shows an image of the character "A" addressed on BTO:Rh/LC device at the beginning of the process and its time evolution at 50 and 100 ms. The response time of the hybrid device is limited by the response of the LC molecules (100–150 ms) since the response of BTO:Rh crystal is much faster (20–30 ms) at the near infrared spectral range [21].

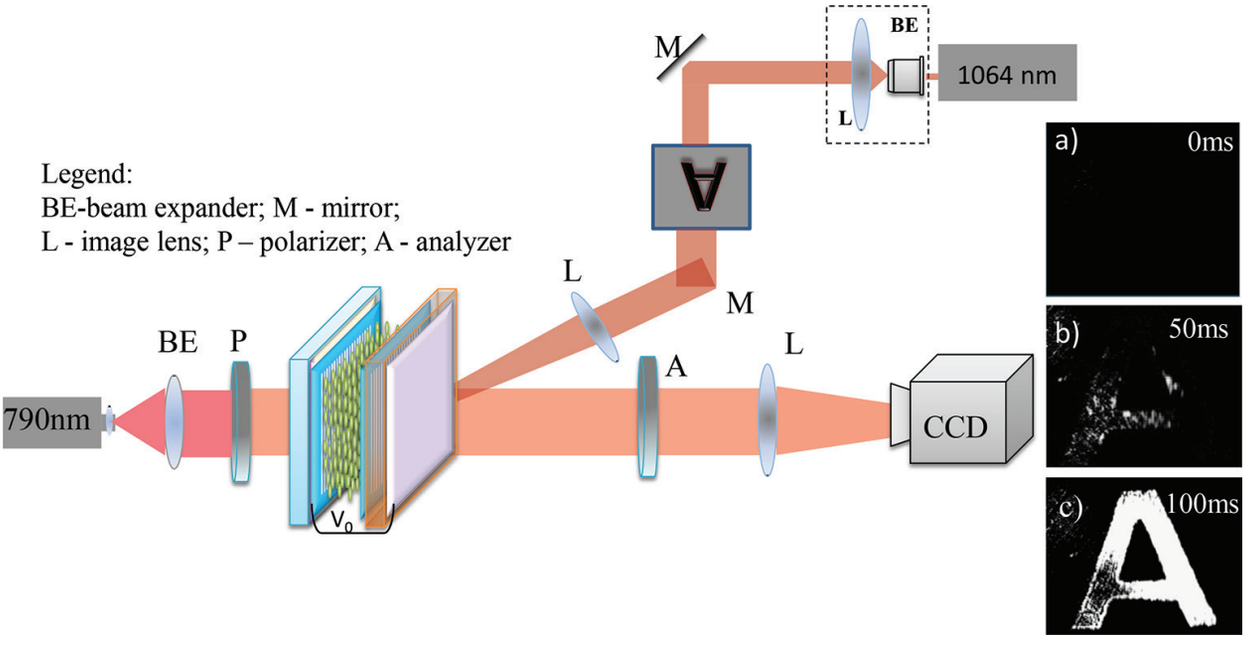

Figure 6. Optical setup for modulated pump light intensity demonstration in BSO:Ru/LC device with graphene electrodes using 1064-nm pump light.

Besides display applications, the Raman-Nath diffraction with multiple output order beams has been successfully applied to control the fast and slow components of light propagation [36]. Different group delays have been obtained depending on the output order and frequency detuning between the pump and signal beam. Varieties of applications in interferometry, optical signal processing, precision metrology and optical sensing are demonstrated [33–37].

5. Organic-inorganic hybrid structures operating at Bragg matched regime of diffraction

5.1. Organic-inorganic hybrid structure design and principle of operation

For most practical realizations, the organic-inorganic structures required to operate at the Bragg matched regime of diffraction, for which the phase matching conditions are satisfied only in one direction. It turns out that selected inorganic photorefractive crystals possesses sufficiently large effective trap density to support efficient space-charge generation necessary to reach the Bragg regime (in comparison with conventional LC cell where the low trap density of LCs is the limitation). In Bragg regime of diffraction, the grating period Λ is comparable with the LC layer thickness ($\Lambda \sim L$) and the hybrid structure acts as a dynamic thick grating.

Generally, this kind of hybrid structure is assembled by photorefractive crystal substrate and a glass substrate, arranged into a cell, filled with liquid crystal or polymer-dispersed liquid crystal layer (PDLC consists of micron-sized droplets of LC molecules randomly dispersed in transparent polymer matrix [38]). The fabrication procedure is very simple and easy, without necessity of conductive layers deposition (external voltage application (and in case of PDLC no need of alignment layers and polarizers)) in contrast to the previously reported devices in Section 4.

The operation principle relays on the unique property of surface-activated photorefractive effect: the photo-generated charge carriers (inside the inorganic substrate) induce a space-charge field, which penetrate into the LC layer and interact with the LC nematic $\hat{n}_{LC}$ director. As a result, the refractive index of LC layer changes which control the light-intensity distribution by producing the diffraction grating. In this hybrid configuration, the two-beam coupling happens at both the photorefractive substrate and LC layer where the charge migration, trap density and space-charge field come from the crystal substrate, whereas the high-beam amplification is provided by the LC layer. Hence, all the processes are controlled only by the action of light.

First, Tabiryan and Umeton theoretically proposed the idea about the surface-localized electromagnetic field in organic-inorganic hybrid structures [39]. In their concept, the photo-generated evanescent electric field combines with the LC director through the LC anisotropy. This electric space charge field plays the essential role as it acts as a driving force for LC molecules re-orientation and subsequent refractive index modulation. **Figure 7** shows the schematic presentation of the above idea.

After Tabiryan and Umeton prediction [39], detailed theory of the beam energy exchange was developed by Jones and Cook [40], according to which the coupling between the space charge field and LC director is caused by the LC static dielectric anisotropy. It predicts that maximal beam coupling occurs when the grating spacing has similar order as LC thickness; however,

http://dx.doi.org/10.5772/67190

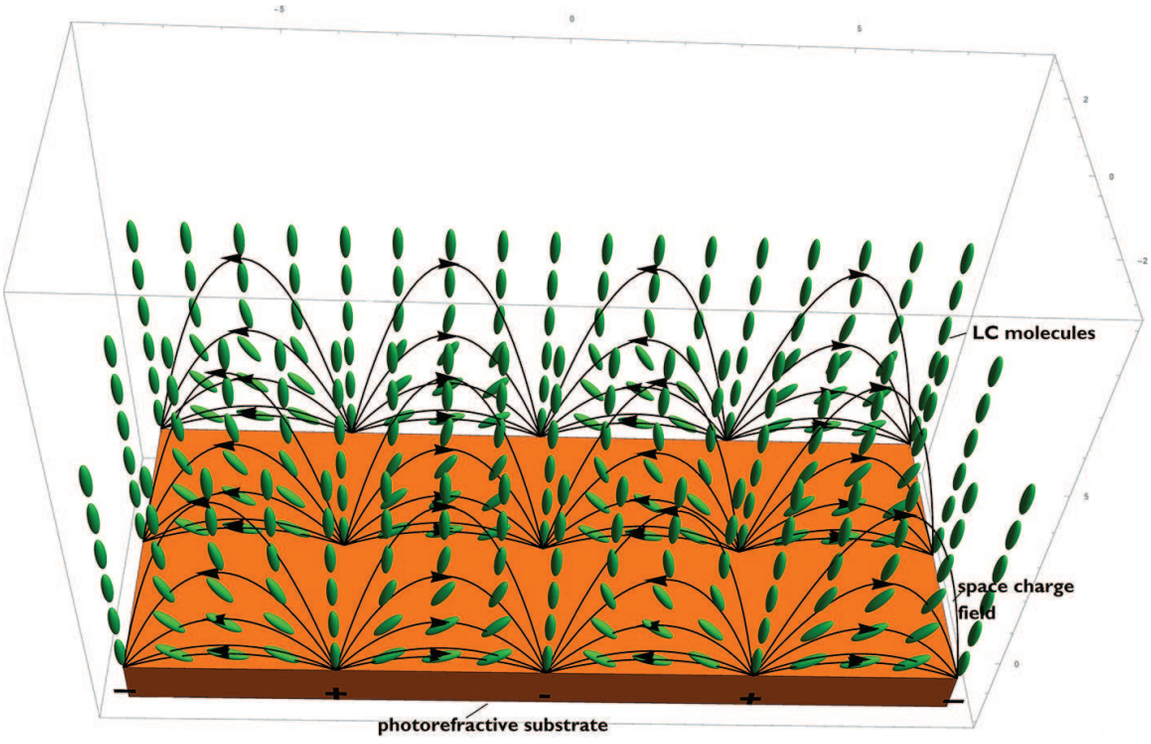

Figure 7. Surface activated photorefractive phenomena [41]. The photo-induced space charge field (indicated with arrows) penetrates into the LC layer and reorient the LC molecules, resulting in a change of the effective refractive index.

experimentally, the maximum coupling happens at much smaller grating spacing than the LC thickness [40]. Later on, Reshetnyak et al. [41] extend the theory summarizing that the exponential gain amplification is a final product of three main components: (i) the beam interference term, (ii) the flexoelectric polarization term of LC (that have upper contribution than the LC static dielectric anisotropy, assumed in Ref. [40]) and (iii) the photo-induced space-charge term. In addition, Evans and Cook [42] performed systematic study and initiate the two necessary conditions to achieve the two-beam coupling at Bragg regime: the LC molecules must be pretilted (asymmetrically aligned) and the LC electrical polarity must be sensitive to the direction of the space-charge field. These conditions enable the refractive index grating to have the same spatial frequency as the interference pattern and make the optical amplification at Bragg regime possible. Afterward, several hybrid configurations based on ferroelectric crystals as $KNbO_3$ and SBN:Ce assembled with nematic LCs, operating at visible spectral range has been realized [42, 43]. For example, Deer [44] demonstrated a structure based on LC layer and $KNbO_3$ substrate, at large beam intersection angle with perfect phase shift between the interference and refractive index gratings. Up to now, only limited numbers of near infrared sensitive structures are designed using semiconductor substrates as CdTe or GaAs. The maximum gain coefficient reported in GaAs/LC cell is 18 cm^{-1} at $\Lambda = 1.2$ μm and 16 cm^{-1} at $\Lambda \sim 1$ μm for CdTe/LC cell, both of them operating at 1064 nm [45, 46].

Figure 8 shows the formation of the space-charge field in BSO:Rh/LC structure followed by monitoring the time evolution of the Gaussian laser beam (0.5-mm waist) propagating through the hybrid device (right side) [47]. Owing to the near-infrared absorption and high

photoconductivity of the inorganic crystal, illumination with 1064-nm light causes charge carriers generation and formation of photo-induced space-charge field which becomes stronger at the edges of the Gaussian beam.

The numerical simulation of the intensity (I) and the space-charge field (E_{sc}) distributions, as well as time evolution of Gaussian beam shape passing through the hybrid structure are shown at **Figure 8**(**b** and **c**). The experimental results are in good agreement with the numerical calculations reported by Stevens and Banerjee [48], which support that Gaussian beam illumination generates notch width which is proportional to the width of the intensity

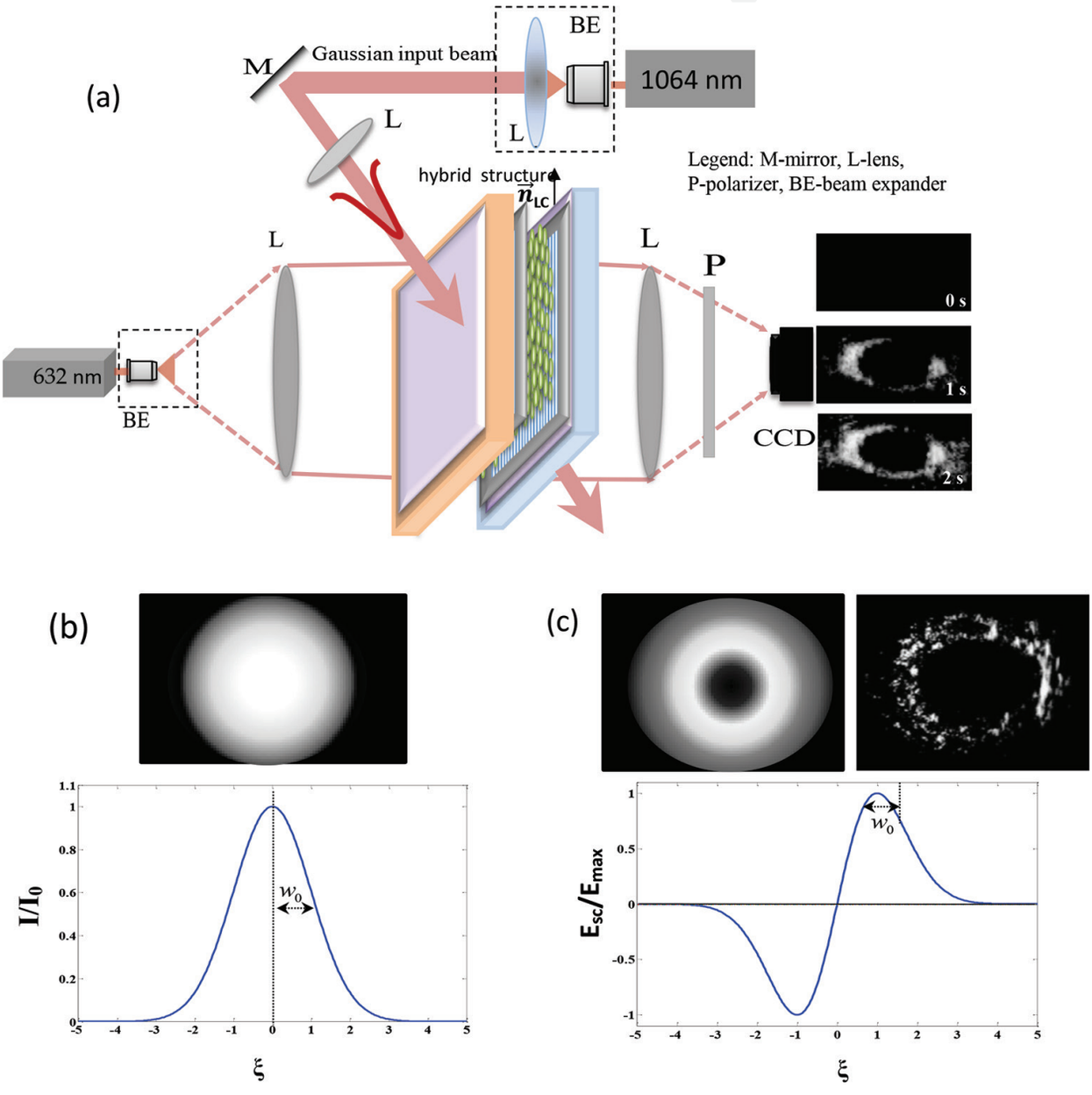

Figure 8. The numerical simulation of the Gaussian intensity beam distribution (a) Gaussian beam propagation through BTO:Rh/LC structure, (b) light intensity numerical distribution and (c) space charge field E_{sc} numerical distribution (left) and experimental propagation of the Gaussian beam (right) through the BSO:Ru/PDLC device.

beam, created by the charge accumulation at the interface between the dark and spurious illumination.

5.2. Two-beam coupling and Bragg-matched regime of diffraction

The evidences of the space charge formation give rise for two-wave mixing experiments. Illumination with two beams leads to light-intensity interference pattern, which induces a space charge field in the photorefractive substrate expressed by [1, 41]:

$$E_{sc} = \frac{i E_D}{1 + \frac{E_D}{E_q}} \tag{19}$$

where $E_D = K\frac{k_B T}{e}$ is the diffusion field, $E_q = \left(1 - \frac{N_A}{N_D}\right)\frac{e N_D}{\epsilon_0 \epsilon_{PR} K}$ is the saturation field and ε_{PR} is the dielectric permittivity of the photorefractive substrate.

Once accumulated in the photorefractive layer, the space-charge field E_{sc} penetrates into the LC layer with decaying evanescent component. In fact, the role of the E_{sc} is to generate electric field, which reorients the nematic LC director $\hat{n}_{LC}$ outside the photorefractive region. Following the couple-wave theory [1, 11], the total electric field obeys the Poisson equation:

$$\nabla .\left(\varepsilon\, \varepsilon_0 . E_{sc} + P_{flex}\right) = 0 \tag{20}$$

where P_{flex} is the flexo-polarization term of LC layer, determined by flexo-electric coefficients according to Refs. [40, 41]. To solve Eq. (20), the authors in Ref. [43] use the relation between the electrical potential in photorefractive substrate $E(x, z)$ and the electrical potential in LC layer $\Psi_{LC}(x, z)$ expressed by $E(x,z) = -\nabla\, \Psi_{LC}(x,z)$ and the boundary conditions between the $z = -L/2$ to $z = L/2$ planes (where L is the LC thickness). Detailed analysis and analytical solutions have been discussed and presented in Refs. [40–43].

The ability of organic-inorganic structures to operate at Bragg match regime of diffraction is shown at **Figure 9** where two hybrid configurations are discussed: the first one is based on Rh-doped $Bi_{12}TiO_{20}$ crystal and LC layer (BTO:Rh/LC), and the second one consists of Ru-doped $Bi_{12}SiO_{20}$ crystal and PDLC layer (BSO:Ru/PDLC). Examples of simultaneously detected behaviour of two interacting beams (linearly polarized with equal intensity [1:1 ratio]) inside the hybrid structures are shown at **Figure 9(b)** and **(c)**, respectively. As it is seen, during the two-wave mixing, a constructive and deconstructive interference occurs, which is indication for $\pi/2$ phase shift between the light pattern and the index grating pattern. In case of BSO:Ru/PDLC structure at the beginning of the light illumination, the two beams propagate together since the PDLC layer requires time to reverse its scattering state to the transparent state and after few seconds clear depletion between two beams appear. No changes between the two interfering beams were detected on glass/LC/glass and glass/PDLC/glass reference samples.

The photo-induced space charge field E_{sc} in the photorefractive substrate has been estimated assuming sinusoidal charge density distribution [1] and materials parameters from **Table 1**. By using Eq. (19), the space charge field in BSO:Ru has been estimated as a value of $E_{sc(BSO:Ru)} = 1.6 \times 10^5$ V/m. Taking into account the experimentally measured threshold

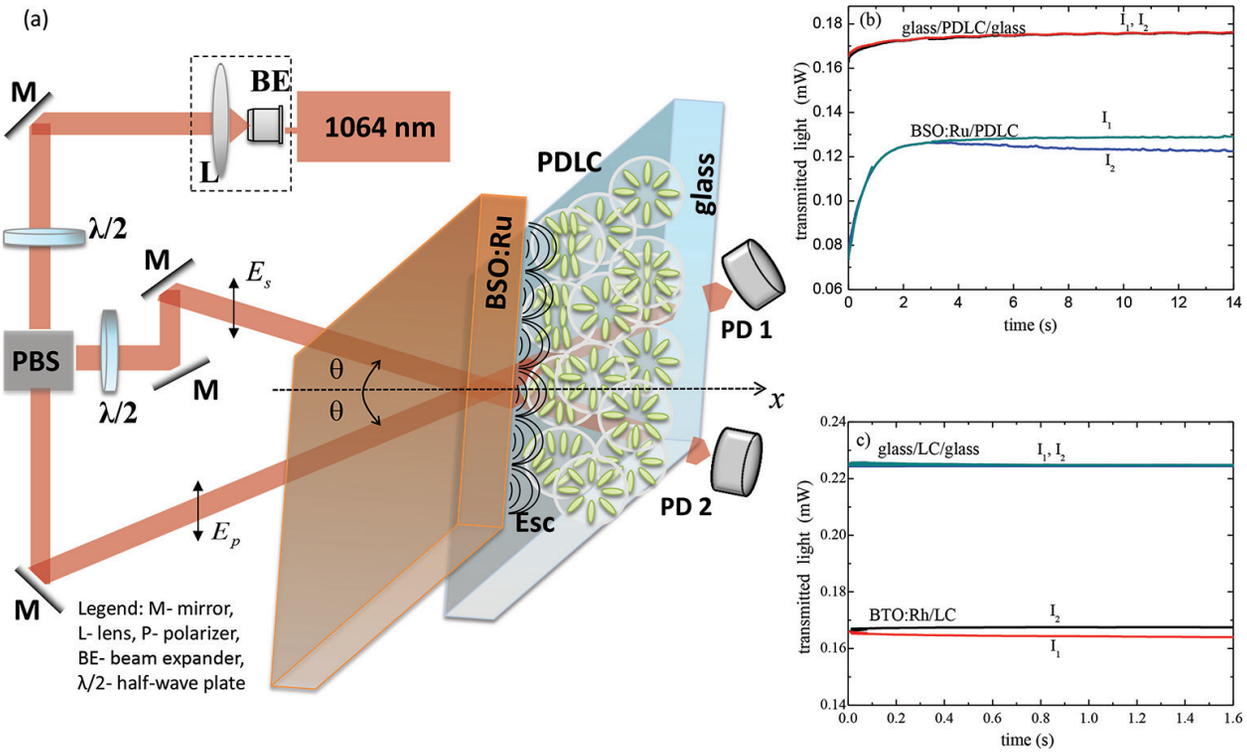

Figure 9. (a) Two-beam coupling experiment in BSO:Ru/PDLC structure and simultaneous behavior of both transmitted beams through the (b) BSO:Ru/PDLC structure and (c) BTO:Rh/LC structure. Comparison with the reference samples as glass/LC/glass and glass/PDLC/glass is also presented.

Type	Symbol	Value	Unit	
LC (MLC type)	$\Delta\varepsilon$ (LC)	41.6 × ε_0		Anisotropy of NLC's dielectric constant
	K (LC)	5		Elastic constant of NLC
	n_0 (LC)	1.51		O-ray refractive index of LC (nematic)
	n_e (LC)	1.75		E-ray refractive index of LC (nematic)
BTO:Rh and BSO:Ru inorganic crystals	N_D	2×10^{24} for BTO:Rh 6.1×10^{23} for BSO:Ru	cm^{-3}	Donor concentration
	N_A	1×10^{24} for BTO:Rh 5×10^{23} for BSO:Ru	cm^{-3}	Acceptor concentration
	ε	46		Dielectric constant of BTO and BSO crystal
	T	300	K	Temperature

Table 1. Material parameters for theoretical simulations.

voltage of 20 V (for 7.3-μm droplet size) of PDLC layer, the threshold electric field is $E_{th(PDLC)} = 2 \times 10^6$ (V/m). Substituting the known values into the boundary condition $E_{sc(BSO:Ru)} \times \varepsilon_{(BSO)} = E_{sc(PDLC)} \times \varepsilon_{(PDLC)}$, we found the required electric field to re-orient LC molecules in PDLC layer is $E_{sc(PDLC)} = 1.25 \times 10^5$ (V/m). Obviously, the generated E_{sc} field inside BSO:Ru substrate is strong enough to penetrate into the PDLC layer and realign the LCs molecules.

For BTO:Rh/LC structure, similar procedure has been performed. The estimated space charge field in BTO:Rh substrate is about $E_{sc(BTO:Rh)} = 1.9 \times 10^5$ (V/m). Taking into account the experimentally measured driving voltage of LC layer as 2 V (for 12-μm thickness) and the threshold electric field as $E_{th(LC)} = 1.67 \times 10^5$ (V/m), the required space charge field is about $E_{sc(LC)} = 1.5 \times 10^5$ (V/m).

The above two examples verify that the photo-induced space charge field E_{sc} created in photorefractive substrates can grow high enough to exceed the threshold electric field and penetrate into the birefringent layer. The advantage of using PDLC over the LC is no need of alignment layer (since the polymer binder defines the droplets orientations), which permits the photo-generated space-charge field to penetrate directly into the PDLC layer.

Figure 10 shows the experimentally measured gain coefficient Γ (cm^{-1}) dependence on the grating spacing Λ (μm) when the ratio of signal-to-pump beam is 1/70. Besides, **Figure 10** shows the theoretically simulated strength of the space-charge field E_{sc} displayed as a single line. For BSO:Ru/PDLC structure, the measured beam amplification value of Γ = 45 cm^{-1} is almost three times higher than reported for similar hybrid structures using double-side photorefractive substrates as CdTe (16 cm^{-1}) and GaAs (18 cm^{-1}), operating at near infrared spectral range [46, 47]. In case of BTO:Rh/LC structure, Γ reached almost 10 cm^{-1} at 1-μm grating spacing. It is assumed that large amplification effect comes from suitable doping elements (as Ru and Rh) addition in sillenite crystal structure, which provides enough density of trap levels to support accumulation of high-resolution space charge field.

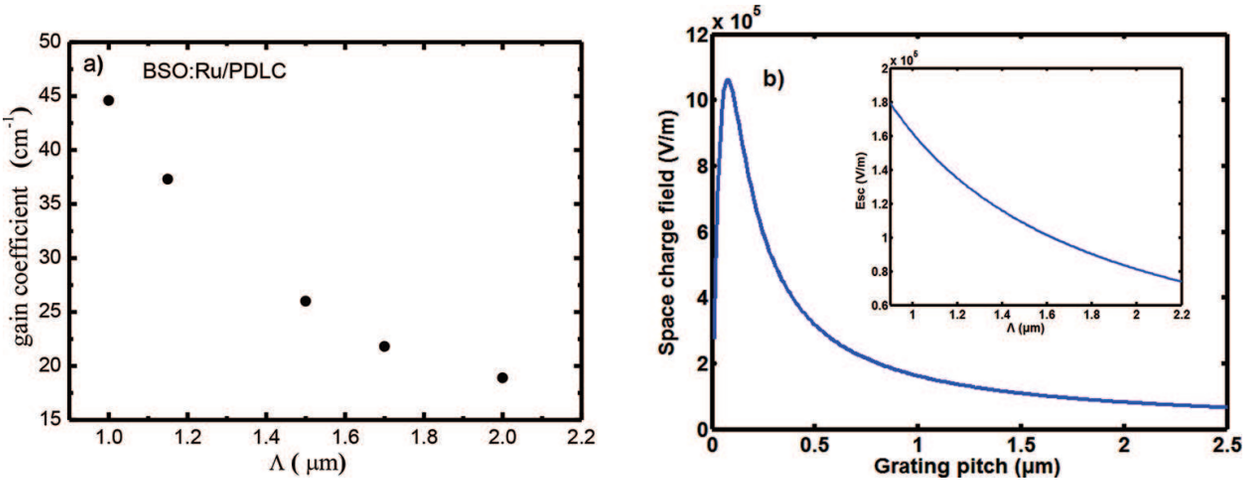

Figure 10. (a) Gain coefficient dependence on the grating spacing Λ(μm) and (b) Theoretical simulation of E_{sc} dependence on Λ(μm) for BSO:Ru/PDLC structure.

As discussed earlier, the Debye screening length in photorefractive material need to be very small to support high concentration of effective trap density. For BSO:Ru crystal, the Debye screening length of 0.08 μm has been calculated from Eq. (7) and materials parameters in **Table 1.** Moreover, as shown in **Figure 10**, the E_{sc} decreases with increasing the grating spacing from 1 to 2 μm. As the gain amplification is controlled by the space charge field, it follows the behaviour of the E_{sc} on the way to decrease with increasing the grating spacing Λ. In that aspect, multi-layer structure may increase the effective interaction length and optimize the E_{sc} penetration depth (however limited by scattering losses).

5.3. Applications

The prime significance of the reviewed hybrid structure is all optically controlled processes. For example, the switching ability BSO:Ru/PDLC structure is demonstrated at **Figure 11**. An image pattern (rectangular mask) is placed into the input plane of 4-f optical system, and the structure is illuminated with 1064-nm Gaussian beam. When the pump light illuminates the device, the PDLC layer transparency is changed due to the induced space charge field in the photorefractive substrate.

Therefore, by controlling the droplet size and consequently the driving voltage of the LC molecules from one side and optimizing the charge carriers' concentration in crystal matrix (providing high enough density for high resolution space charge field), the proposed structure can be further optimized. Moreover, the beam coupling can be significantly improved by addition of nanoparticles in LC layer, which affects the dielectric anisotropy and decreases the driving (threshold) voltage.

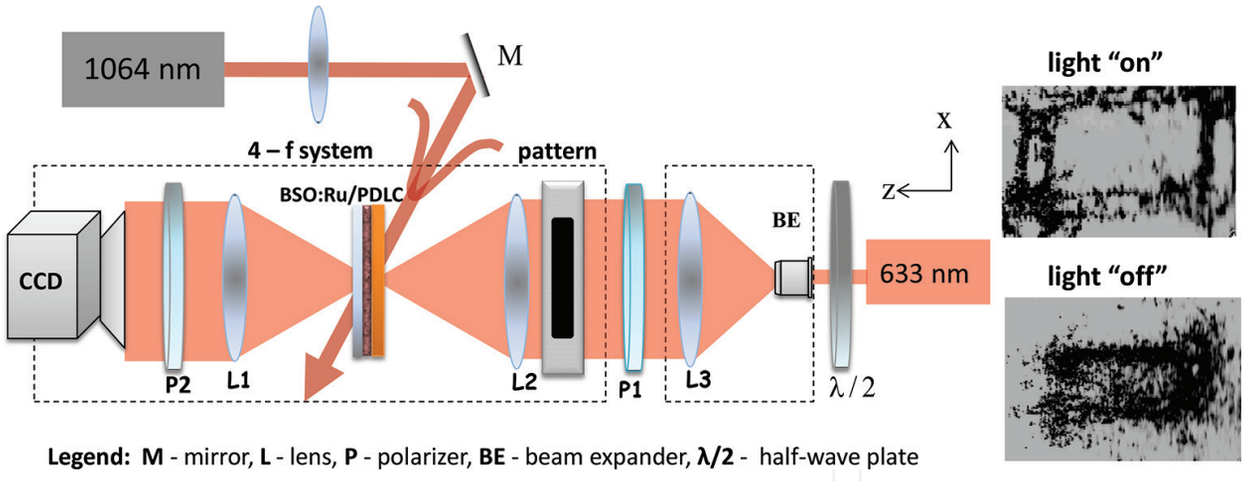

Figure 11. Gaussian laser beam propagating through BSO/PDLC hybrid structure and image mask (rectangular shape) evolution when the light is at "on" and "off" position (right side). All processes are controlled by near infrared light only.

6. Conclusion

The chapter reviewed recent progress of two-wave mixing and beam amplification in novel type of hybrid structures that combine photoconductive and photorefractive properties of

http://dx.doi.org/10.5772/67190

inorganic crystals together with the high birefringence and anisotropy of LC (or PDLC) layers. When inorganic crystal acts as photoconductive substrate, the photo-generated charge carriers control the LC molecules alignment and subsequent light modulation. As a result, the two-wave mixing happens in a liquid crystal layer (the active layer) with high amplification values; however, the fringe period of the recorded gratings is limited to few micrometers. When inorganic crystal acts as photorefractive substrate, the two-beam coupling happens at both the photorefractive substrate and LC layer where the space charge field is the driving force for LC molecules reorientation and refractive index modulation. In this configuration, all the processes are controlled by light-permitting submicron resolution.

Depending on the designed structure assembly and operation principle, dynamic holographic gratings at Raman-Nath or Bragg match regimes of diffraction can be recorded. The large trap density and small grating spacing typical for photorefractive materials allow to reach the Bragg matched conditions in all optically controlled structure in contract to the large grating spacing and small trap density typical for LC-based electro-optically controlled structures, which support the Raman-Nath regime of diffraction. Furthermore, by selecting the photosensitivity of inorganic substrate, the spectral interval can be easily adjusted in a regions, where the LC molecules (or PDLC) are not enough sensitive.

The proposed organic-inorganic hybrid structures can control transmission, reflection and scattering of light and are considered in playing an essential role in 3D holographic display technologies and providing sub-micron spatial resolution, large viewing angle and low driving voltage. The reviewed examples can be classified as novel type of non-linear optical components, which exhibit attractive capabilities for light manipulation, coherent image amplification, to control the group velocity of modulated signal beam, in video display technologies. The advantage of simple fabrication and compactness open the way to design varieties of new structures and elements that meet the up-to-date requirements of 3D display technologies and optical information processing.

Acknowledgments

Financial support by the Ministry of Science and Technology, Taiwan under the contracts: MOST 105-2221-E-009-110; 104-2221-E-009-164; 104-2221-E-009-151 and Bulgarian Science Fund under the projects DFNI T-02/26 and H-08/9 are gratefully acknowledged.

Author details

Vera Marinova[1,2]*, Shiuan Huei Lin[3] and Ken Yuh Hsu[1]

*Address all correspondence to: veramarinova@nctu.edu.tw

1 Photonics Department, National Chiao Tung University, Taiwan

2 Institute of Optical Materials and Technologies, Sofia, Bulgaria

3 Department of Electrophysics, National Chiao Tung University, Taiwan

References

[1] Yeh P, Gu C. Optics of Liquid Crystal Displays. 2nd ed. New Jersey: Wiley; 2009. 792 p. ISBN: 978-0-470-18176-8

[2] Yeh P. Introduction to Photorefractive Nonlinear Optics. New York: Wiley; 1993. 491 p. DOI: ISBN: 978-0-471-58692-0

[3] Yariv A, Yeh P. Optical Waves in Crystals: Propagation and Control of Laser Radiation. New York: Wiley; 2002. 604 p. DOI: ISBN: 978-0-471-43081-0

[4] Toal V. Introduction to Holography. Boca Raton: CRC Press; 2011. 502 p. DOI: ISBN: 9781439818688

[5] Klein WR, Cook BD. Unified approach to ultrasonic light diffraction. IEEE Trans Sonics Ultrason. 1967;**SU-14**(3):123–134.

[6] Moharam MG, Young L. Criterion for Bragg and Raman-Nath diffraction regimes. Appl Optics. 1978;**17**(11):1757–1759. DOI: 10.1364/AO.17.001757

[7] Gunter P, Huignard JP, editors. Photorefractive Materials and their Applications I. Berlin: Springer-Verlag; 1988. 441 p.

[8] Yeh P. Two-wave mixing in non-linear media. IEEE J Quant Electron. 1989;**25**(3):484–519. DOI: 10.1109/3.18564

[9] Chi M, Huignard JP, Petersen PM. A general theory of two-wave mixing in non-linear media. J Opt Soc Am B. 2009;**26**(8):1578–1584. DOI: 10.1364/JOSAB.26.001578

[10] Nolte DD, editor. Photorefractive Effects and Materials. New York: Springer Science + Business Media; 1995. 494 p.

[11] Kogelnik N. Coupled wave theory for thick hologram gratings. Bell Syst Tech J. 1969;**48**:2909–2947.

[12] Blanche PA, editor. Photorefractive Organic Materials and Applications. Switzerland: Springer; 2016. 325 p. DOI: 10.1007/978-1-4615-2227-0

[13] Ostroverkhova O, Moerner WE. Organic photorefractives: mechanism, materials and applications. Chem Rev. 2004;**104**:3267–3313. DOI: 10.1021/cr960055c

[14] Kajzar F, Bartkiewicz, Miniewicz A. Optical amplification with high gain in hybrid polymer-liquid-crystal structures. Appl Phys Lett. 1999;**74**(20):2924–2926. DOI: 10.1063/1.123967

[15] Buse K. Light-induced charge transport properties in photorefractive crystals II: materials. Appl Phys B. 1997;**64**:391–407. DOI: 10.1007/s003400050190

[16] Frejlich J. Photorefractive Materials: Fundamental Concepts, Holographic Recording and Materials Characterization. New York: Wiley Interscience; 2007. 336 p. DOI: 10.1002/0470089067

[17] Marinova V, Hsieh ML, Lin SH, Hsu KY. Effect of ruthenium doping on the optical and photorefractive properties of $Bi_{12}TiO_{20}$ single crystals. Opt Comm. 2002;**203**(3–6):377–384. DOI: 10.1016/S0030-4018(02)01127-6

[18] Marinova V, Liu RC, Lin SH, Hsu KY. Real time holography in ruthenium doped bismuth sillenite crystals at 1064 nm. Opt Lett. 2011;**36**(11):1981–1983. DOI: 10.1364/OL.36.001981

[19] Marinova V, Liu RC, Chen MS, Lin YH, Lin SH, Hsu KY. Near infrared properties of Rh-doped $Bi_{12}TiO_{20}$ crystals for photonic applications. Opt Lett. 2013;**38**:495–497. DOI: 10.1364/OL.38.000495

[20] Liu RC, Marinova V, Lin SH, Chen MS, Lin YH, Hsu KY. Near infrared sensitive photorefractive device using PDLC and BSO:Ru hybrid structure. Opt Lett. 2014;**39**:3320–3323. DOI: 10.1364/OL.39.003320

[21] Marinova V, Liu RC, Lin SH, Chen MS, Lin SH, Hsu KY. Near infrared sensitive organic–inorganic photorefractive device. Opt Rev. 2016;**23**(5):811–816. DOI: 10.1007/s10043-016-0249-z

[22] Marinova V, Chi CH, Tong ZF, Berberova N, Liu RC, Lin SH, Lin YH, Stoykova E, Hsu KY. Liquid crystal light valve operating at near infrared spectral range. Opt Quant Electron. 2016;**48**:270. DOI: 10.1007/s11082-016-0546-6

[23] Aubourg P, Huignard JP, Hareng M, Mullen RA. Liquid crystal light valve using bulk monocrystalline $Bi_{12}SiO_{20}$ as the photoconductive material. Appl Opt. 1982;**21**:3706–3712. DOI: 10.1364/AO.21.003706

[24] Residori S, Bortolozzo U, Huignard JP. Slow light using wave mixing in liquid crystal light-valves. Appl Phys B. 2009;**95**:551–557. DOI: 10.1007/s00340-009-3556-2

[25] Bortolozzo U, Residori S, Huignard JP. Beam coupling in photorefractive liquid crystal light valves. J Phys D. 2008;**41**:224007. DOI: 10.1088/0022-3727/41/22/224007

[26] Huignard JP. Spatial light modulators and their applications. J Opt. 1987;**18**:181–186. DOI: 10.1088/0150-536X/18/4/003

[27] Luo S, Wang Y, Tong X, Wang Z. Graphene based optical modulators. Nanoscale Res Lett. 2015;**10**:199. DOI: 10.1186/s11671-015-0866-7

[28] Jung YU, Park KW, Hur ST, Choi SW, Kang SJ. High transmittance liquid-crystal displays using graphene conducting layers. Liq Cryst. 2014;**41**:101–105. DOI: 10.1080/02678292.2013.837517

[29] Fukushima S, Kurokawa T, Ohno M. Real-time hologram construction and reconstruction using a high-resolution spatial light modulator. Appl Phys Lett. 1991;**58**:787–789. DOI: 10.1063/1.104516

[30] White DL, Feldman M. Liquid-crystal light valves. Electron Lett. 1970;**6**:837–839. DOI: 10.1049/el:19700578

[31] Khoo C. Liquid Crystals Physical Properties and Nonlinear Optical Phenomena. 2nd ed. New York: Wiley; 1996. 369 p. DOI: 10.1002/0470084030

[32] Brignon A, Bongrand I, Loiseaux B, Huignard JP. Signal-beam amplification by two-wave mixing in a liquid-crystal light valve. Opt Lett. 1997;**22**(24):1855–1857. DOI: 10.1364/OL.22.001855

[33] Shcherbin K, Gvozdovskyy I, Evans RD. Optimization of the liquid crystal light valve for signal beam amplification. Opt Mat Express. 2016;**6**(11):3670–3675. DOI: 10.1364/OME.6.003670

[34] Bortolozzo U, Residori S, Huignard JP. Transmissive liquid crystal light-valve for near-infrared applications. Appl Opt. 2013;**52**:E73–E77. DOI: 10.1364/AO.52.000E73

[35] Peigine A, Botrolozzo U, Residori S, Molin S, Nouchi P, Dolti D, Huignard JP. Adaptive holographic interferometer at 1.55 μm based on optically addressed spatial light modulator. Opt Lett. 2015;**40**(23):5482–5485. DOI: 10.1364/OL.40.005482

[36] Bortolozzo U, Residori S, Huignard JP. Slow and fast light: basic concepts and recent advancements based on nonlinear wave-mixing processing. Laser Photon Rev. 2009;**4**(4):483–498. DOI: 10.1002/lpor.200910022

[37] Bortolozzo U, Residori S, Huignard JP. Adaptive holography in liquid crystal light valves. Materials. 2012;**5**:1546–1559. DOI: 10.3390/ma5091546

[38] Coates D. Polymer-dispersed liquid crystals. J Mater Chem. 1995;**5**:2063–2072. DOI: 10.1039/JM9950502063

[39] Tabiryan NV, Umeton C. Surface-activated photorefractivity and electro-optic phenomena in liquid crystals. J Opt Soc Am B. 1988;**15**:1912–1917. DOI: 10.1364/JOSAB.15.001912

[40] Jones DC, Cook G. Theory of beam coupling in a hybrid photorefractive liquid crystal cells. Opt Commun. 2004;**232**:399–409. DOI: 10.1016/j.optcom.2003.12.050

[41] Reshetnyak VY, Pinkevych IP, Cook G, Evans DR, Sluckin TJ. Two-beam energy exchange in a hybrid photorefractive-flexoelectric liquid crystal cell. Phys Rev E. 2010;**81**:031705. DOI: 10.1103/PhysRevE.81.031705

[42] Evans DR, Cook G. Bragg-matched photorefractive two-beam coupling in organic-inorganic hybrids. J Nonlinear Optic Phys Mat. 2007;**16**:271–280. DOI: 10.1142/S0218863507003767

[43] Cook G, Carns JL, Saleh MA, Evans DR. Substrate induced pre-tilt in hybrid liquid crystal/inorganic photorefractive. Mol Cryst Liq Cryst. 2006;**453**:141–153. DOI: 10.1080/15421400600651591

[44] Deer MJ. Demonstration of an Fe-doped $KNbO_3$ photorefractive hybrid. Appl Phys Lett. 2006;**88**:254107. DOI: 10.1063/1.2214173

[45] Garcia RR, Rodriguez CB. Enhancement of the coupling gain in GaAs-liquid crystal hybrid devices. Mol Cryst Liq Cryst. 2012;**561**:68–73. DOI: 10.1080/15421406.2012.686713

[46] Gvozdovskyy I, Shcherbin K, Evans DR, Cook G. Infrared sensitive liquid crystal photorefractive hybrid cell with semiconductor substrate. Appl Phys B. 2011;**104**:883–886. DOI: s00340-011-4374-x

[47] MarinovaV, Liu RC, Chen MS, Lin SH, Lin YH, Hsu KY. All optically controlled light valve assembled by photorefractive crystal and PDLC hybrid structure. Proc SPIE. 2015;**9508**:95080O. DOI: 10.1117/12.2178985

[48] Stevens DM, Banerjee PP. Gaussian-beam-induced photorefractive birefringence and its application to radio-frequency signal excision. Opt Lett. 2002;**27**:1333–1335. DOI: 10.1364/OL.27.001333

IntechOpen